

# Journal of Materials Chemistry B

Accepted Manuscript



This article can be cited before page numbers have been issued, to do this please use: Y. Huang, N. He, Y. Wang, D. Shen, Q. Kang, R. Zhao and L. Chen, *J. Mater. Chem. B*, 2019, DOI: 10.1039/C8TB03054E.



This is an Accepted Manuscript, which has been through the Royal Society of Chemistry peer review process and has been accepted for publication.

Accepted Manuscripts are published online shortly after acceptance, before technical editing, formatting and proof reading. Using this free service, authors can make their results available to the community, in citable form, before we publish the edited article. We will replace this Accepted Manuscript with the edited and formatted Advance Article as soon as it is available.

You can find more information about Accepted Manuscripts in the [author guidelines](#).

Please note that technical editing may introduce minor changes to the text and/or graphics, which may alter content. The journal's standard [Terms & Conditions](#) and the ethical guidelines, outlined in our [author and reviewer resource centre](#), still apply. In no event shall the Royal Society of Chemistry be held responsible for any errors or omissions in this Accepted Manuscript or any consequences arising from the use of any information it contains.

# Self-assembly Nanoparticles by Human Serum Albumin and Photosensitizer for Targeted Near-infrared Emission Fluorescence Imaging and Effective Phototherapy of Cancer

Received 00th January 20xx,  
Accepted 00th January 20xx

DOI: 10.1039/x0xx00000x

www.rsc.org/

Yan Huang,<sup>a,b</sup> Na He,<sup>b</sup> Yunqing Wang,<sup>b</sup> Dazhong Shen,<sup>a</sup> Qi Kang,<sup>\*a</sup> Rongfang Zhao,<sup>b</sup> Lingxin Chen<sup>\*b,c</sup>

Photodynamic therapy (PDT) and photothermal therapy (PTT) are effective treatment ways for cancer, and the photosensitizer plays the most important role in the treatment. However, the ideal photosensitizers are insufficient for *in vivo* tumor treatment. Herein, we develop a small molecule fluorophore Cy-HPT as a novel photosensitizer, which with the advantages of near-infrared (NIR) emission wavelength, high photothermal conversion efficiency and high singlet oxygen generation efficiency. Moreover, a nanoplatfrom of HSA@Cy-HPT is synthesized by self-assemble of Cy-HPT and human serum albumin (HSA) and Cy-HPT in aqueous solution. Compared to Cy-HPT, HSA@Cy-HPT exhibits not only much stable spectral properties, superior effect of PDT/PTT but also more satisfactory *in vivo* metabolism. HSA@Cy-HPT shows an outstanding tumor targeting feature in subcutaneous tumor xenograft models due to its enhanced permeability and retention effect for tumor tissue. Furthermore, HSA@Cy-HPT is successfully applied to treatment of tumor xenograft models, the tumor tissue is obviously inhibited without any regrowth and extend survival rate of models. Also, the normal tissue of tumor xenograft models is observed no distinct damage by hematoxylin & eosin staining. This work provides a promising therapeutic agent for the synergetic PDT and PTT for cancer.

## 1. Introduction

As the incidence and death rates associated with cancer remain high, the innovated therapeutic strategies are imperative. Conventional treatment of cancers includes combinations of surgery, radiotherapy, and chemotherapy. Photodynamic therapy (PDT) and photothermal therapy (PTT) are the promising therapeutic techniques due to high curative effect, low toxicity and negligible side effects.<sup>1-3</sup> Photosensitizer plays the key role in both PDT and PTT. On one hand, they are generally excited to generate singlet oxygen (<sup>1</sup>O<sub>2</sub>) under light irradiation due to the photophysical conversion phenomena.<sup>4</sup> <sup>1</sup>O<sub>2</sub> not only has an extremely oxidation for the clipping react with protein, free radical and other bioactive molecules in cytoplasm, but also can penetrate the nuclear membrane and lead to DNA damage and some other physiological changes.<sup>4</sup> On the other hand, photosensitizer is also crucial for PTT, which can transform the luminous energy to thermal energy under the laser irradiation. The tumor cells are extremely sensitive to

temperature than normal cells. The local temperature increasing causes DNA damage and the apoptosis of tumor cells eventually.<sup>5</sup> Considering the superiority of PDT and PTT, the synergetic PDT and PTT treatments have been widely used in clinical treatment of tumor.<sup>6-13</sup>

Recently, the design and synthesis of small molecule photosensitizer has been widely reported.<sup>14-16</sup> Some fluorescent dyes have been demonstrated with photosensitization effects, which are closely associated with their lipo-hydro partition coefficients (log P), polarizabilities, and molar absorption coefficients.<sup>17,18</sup> Most of the reported photosensitizers having the excitation and emission wavelengths in visible region, and are not suitable for the imaging and PDT/PTT in deep organization.<sup>19-23</sup> Indocyanine green (ICG) is Food and Drug Administration (FDA)-approved NIR photosensitizer,<sup>24, 25</sup> for clinical application.<sup>26</sup> However, there are several drawbacks such as self-aggregation in physiological solutions, nonspecific binding to proteins, and rapid renal elimination from the body. To address these problems, researchers developed a new ICG analog, IR-DBI, with simultaneous NIR imaging and chemo-/PDT/PTT/multimodal anticancer activity, which has the better treatment than ICG.<sup>18</sup> However, the maximum absorbance (near 780 nm) is still away from the wavelength of common used 808 nm excitation laser, thus affecting the treatment efficacy. Moreover, IR-DBI with a small-molecule structure is difficult to accumulate in tumor tissue within the suitable treatment time. Therefore, the development of ideal photosensitizer with a suitable excitation and emission wavelengths for the effective PDT

<sup>a</sup> College of Chemistry, Chemical Engineering and Materials Science, Key Laboratory of Molecular and Nano Probes, Ministry of Education, Shandong Normal University, Jinan 250014, China. \*E-mail: kangqi@sdsu.edu.cn.

<sup>b</sup> CAS Key Laboratory of Coastal Environmental Processes and Ecological Remediation, The Research Center for Coastal Environmental Engineering and Technology, Yantai Institute of Coastal Zone Research, Chinese Academy of Sciences, Yantai 264003, China. \*E-mail: lxchen@yic.ac.cn.

<sup>c</sup> College of Chemistry and Chemical Engineering, Qufu Normal University, Qufu 273165, China.

†Electronic Supplementary Information (ESI) available: [details of any supplementary information available should be included here]. See DOI: 10.1039/x0xx00000x

and PTT, which could be accumulated in tumor tissue with a reasonable time is necessary.

Photosensitizer loaded, multifunctional nanoplateform also has great importance and interest in a variety of medical applications.<sup>27-32</sup> The rapid development of nanomaterials with large surface areas, tunable material properties, and strong signal output will have significant impact on the future personalized oncology.<sup>33-35</sup> Compared with small-molecule photosensitizer, the nanoplateform has some advantages, such as superior photostability, effective targeting and long-time accumulation in tumor.<sup>36-41</sup> To date, various inorganic and organic nanomaterials (NMs) made of carbon, gold and organic polymer have been applied to PDT and PTT for cancer.<sup>1, 35, 42-44</sup> However, NMs with hydrodynamic diameter ranging from 10 to 200 nm are easy to non-specific accumulation in reticuloendothelial system (RES) organs for a long time, which raises concerns about the long-term risk of adverse effects.<sup>45-47</sup> Recently, protein based theranostics nanoplateforms have been extensively investigated. The self-assemblies between amphiphilic photosensitizers and endogenic proteins (such as human serum albumin, HSA) exhibit high drug loading rates, good water-solubility, biocompatibility, and tumor selectivity.<sup>48-50</sup> Meanwhile, the size (nearly 10 nm) is suitable for renal clearance to eliminate possible accumulation toxicity.<sup>48</sup>

Herein, we report a photosensitizer that benzo-heptamethine cyanine dye triphenylphosphonio benzo cyanine (Cy-HPT), with a longer emission wavelength (860 nm) than previous research,<sup>14</sup> which is benefit for the application of PDT/PTT *in vivo*. Furthermore, we synthesized a nanoplateform HSA@Cy-HPT by self-assembling of Cy-HPT and HSA. This nanoplateform exhibits excellent photostability, tumor cell-selectivity, and satisfactory synergetic PDT/PTT effect *in vitro* and *in vivo* via the efficient photothermal conversion and the generation of <sup>1</sup>O<sub>2</sub> under NIR laser irradiation. Our study indicates that the synergetic PDT and PTT have the distinguished treatment effect for cancer cells. Western blot verified the HSA@Cy-HPT induced apoptosis by quantified the apoptosis related protein. *In vivo* experiments reveal that HSA@Cy-HPT has long-time accumulation in tumor site due to the EPR effect, followed by efficient renal clearance. Finally, the tumor tissue has been obviously inhibited without any regrowth and extend survival rate of models by the PDT and PTT of HSA@Cy-HPT.

## 2. Experimental

### 2.1 Preparation and Characterization of HSA@Cy-HPT

HSA@Cy-HPT were prepared with the similar method previously reported.<sup>48</sup> Briefly, 5 mg as-synthesized Cy-HPT was firstly dispersed in 10 ml methanol. HSA (Sigma-Aldrich, 200 mg) and 10 μL TEA (triethylamine) were mixed in 10 ml ultrapure water for 30 min. Then, the mixture was added with 10 ml above-mentioned methanol solution of Cy-HPT for overnight vigorous stirring. After 24 h dialysis of the reaction solution with a dialysis bag (MWCO 10 KDa), HSA@Cy-HPT nanoparticles were obtained. The mean particle size was determined by DLS Zetasizer Nano ZS90 (Malvern Instruments Ltd, UK) and by TEM (JEOL, model JEM-1230, Japan) operated at 100 kV. The optical properties of chemicals and HSA@Cy-HPT nanoparticles were characterized by using Thermo

Scientific NanoDrop 2000/2000C spectrophotometer, and a NIR fluorescence spectrometer (HORIBA Scientific Fluoromax-4 spectrofluorometer with a Xenon lamp and 1.0-cm quartz cells) with 810 nm excitation and scanning the wavelength from 830 to 900 nm (5-nm slit width at a scan speed of 600 nm/min).

### 2.2 Animals and Tumor Xenografts.

BALB/c mice (aged 5-6 weeks, weighed 20-25 g) and athymic nude mice (aged 5-6 weeks, weighted 20-25 g) were purchased from Binzhou Medical University. All experimental procedures were conducted in conformity with institutional guidelines for the care and use of laboratory animals, and protocols were approved by the Institutional Animal Care and Use Committee in Binzhou Medical University, Yantai, China. For HepG2 tumor xenografts, 5 × 10<sup>6</sup> HepG2 cells suspended in 200 μL PBS were subcutaneously implanted into the right flank of each athymic nude mouse. All animals were maintained under aseptic conditions and were housed in a group of five in standard cages with free access to food and water and a 12 h light/dark cycle.

### 2.3 Tumor NIR Fluorescent Imaging and Thermal Imaging.

The animals with HepG2 tumor xenograft models were used for tumor-targeted NIR imaging after 48 h intravenously injected 10 mg/kg HSA@Cy-HPT with the Perkinelmer IVIS Lumina XRMS Series III In Vivo Imaging System.<sup>5</sup> NIR imaging of whole animals *in vivo* was performed at different times (0.5h, 6 h, 24 h, 48 h, 72 h) post drug injection. After sacrifice of the mice at 0.5 h, 6 h, 24 h, 48 h and 72 h, major organs and tumors were dissected for *ex vivo* NIR fluorescent imaging, and for studying their tissue distribution. For *in vivo* assessment of PTT property, mice with HepG2 tumor xenografts were intravenously injected HSA@Cy-HPT with 10 mg/kg. After 24 h injection, the realtime temperature change of mice was imaged by the infrared thermal camera (Testo 865, Germany) when the whole tumor tissue was exposed to the continuous NIR laser beam (808 nm, 1.5 W/cm<sup>2</sup>, 5 min). Prior to NIR fluorescence or thermal imaging, mice were anesthetized by inhalation of isoflurane.

### 2.4 Synthesis of Compound Cy-HPT

Compound 4 (46.5 mg, 0.05 mmol) and (4-Bromobutyl) triphenylphosphonium bromide (47.8 mg, 0.1 mmol) were dissolved in dry acetone (25 mL), then anhydrous potassium carbonate (27.5 mg, 0.2 mmol) was added. The mixture was stirred under a dry argon atmosphere for 24 h and monitored by TLC. After the reaction was finished, the mixture was cooled to room temperature, evaporated under reduced pressure and partitioned with CH<sub>2</sub>Cl<sub>2</sub> and saturated KBr solution. Finally, the organic layer was separated. Purification by column chromatography on silica eluting with EtOAc/CH<sub>3</sub>OH (3:1) gave the product Cy-HPT as dark green crystals (35.74 mg, 53%). <sup>1</sup>H NMR (CH<sub>3</sub>DO, 500 MHz) δ (ppm): 8.47-8.45 (m, 2H), 7.87-7.76 (m, 6H), 7.63-7.50 (m, 5H), 7.36-7.28 (m, 19H), 7.05-6.91 (m, 5H), 6.37-6.10 (m, 1H), 5.33 (m, 1H), 4.57-4.27 (m, 2H), 4.13-4.03 (m, 2H), 3.87-3.44 (m, 8H), 3.30 (m, 8H), 2.96-2.93 (m, 1H), 2.63-2.62 (m, 2H), 2.18-2.09 (m, 4H), 1.94-1.88 (m, 8H), 1.76-1.62 (m, 4H), 1.28 (m, 6H), 0.89 (m, 2H). <sup>13</sup>C NMR (CH<sub>3</sub>DO, 125 MHz) δ (ppm): 175.7, 171.5, 165.4, 165.1, 160.6, 137.5, 133.4, 132.0, 131.9, 131.8, 129.8, 129.0, 128.7, 128.6, 128.5,

126.3, 117.3, 113.7, 113.6, 112.4, 112.3, 49.7, 49.6, 49.5, 49.2, 46.7, 46.5, 46.4, 46.2, 46.0, 45.9, 45.7, 45.5, 42.6, 30.1, 27.8, 27.5, 27.4, 25.3, 25.1, 25.0, 24.8, 18.4. LC-MS (ESI<sup>+</sup>): m/z C<sub>88</sub>H<sub>86</sub>ClN<sub>4</sub>O<sub>7</sub>P<sup>2+</sup> calcd. 674.29, found [M<sup>+</sup>] 674.69.

### 3. Results and discussion

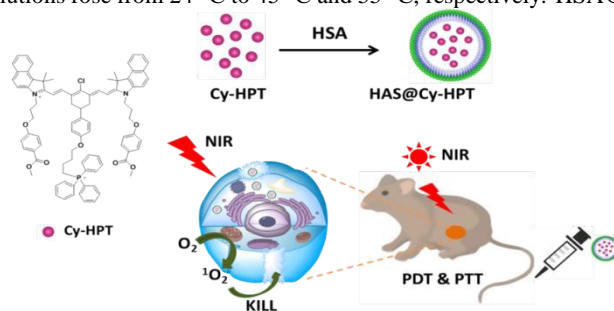
#### 3.1 Synthesis and Characterization of Cy-HPT and HSA@Cy-HPT

A benzo-heptamethine cyanine dye by modification of N-alkyl side chains based on the heptamethine core was designed and synthesized, and was named Cy-HPT (Scheme 1). Structures of the Cy-HPT were characterized by <sup>1</sup>H NMR, <sup>13</sup>C NMR, and mass spectrometry (MS), as described in Supporting Information. HSA@Cy-HPT nanoparticle (NP) was synthesized by the self-assembly of Cy-HPT and HSA (Scheme 1). Cy-HPT can be adsorbed onto the hydrophobic domain of HSA, the complex with much higher hydrophobicity can act as an “adhesive” between different proteins, and then induce assembly of more albumin proteins to form a nanoparticle, inside which Cy-HPT are embedded. We then carefully characterized the obtained HSA@Cy-HPT nanoparticles. The HSA@Cy-HPT we obtained had the loading ratio of 6.7% for Cy-HPT. Transmission electron microscopy (TEM) imaging and DLS analysis revealed that the size of NP was around 10 nm, indicating that the Cy-HPT binding dose not induce severe HSA aggregation (Fig. 1a and 1b). The NPs could be easily dispersed in various physiological buffers. The different pH effects on Cy-HPT and HSA@Cy-HPT were investigated in Supporting Information (Fig. S1).

The spectroscopic properties of the Cy-HPT and HSA@Cy-HPT were investigated under simulated physiological conditions (10 mM HEPES pH 7.4). As shown in Fig. 1c, the maximum absorption of Cy-HPT and HSA@Cy-HPT appeared at 830 nm ( $\epsilon_{830\text{ nm}} = 4.2 \times 10^4 \text{ M}^{-1} \text{ cm}^{-1}$ ) and 833 nm ( $\epsilon_{833\text{ nm}} = 7.9 \times 10^4 \text{ M}^{-1} \text{ cm}^{-1}$ ), respectively. The Cy-HPT and HSA@Cy-HPT exhibited fluorescence emission spectra centered at 860 nm and 863 nm, respectively, which extended across the NIR region (Fig. 1d). The modification of N-alkyl side chains based on the heptamethine core might make the long emission wavelength. Due to extremely low tissue autofluorescence and absorption in NIR spectral range (650 - 900 nm), optical imaging and phototherapy with high sensitivity and deep tissue penetration could be realized. It should be noted that HSA@Cy-HPT exhibited slightly red-shifted absorbance and emission peak as well as obviously enhanced fluorescence compared with Cy-HPT (Fig. 1d), which are likely owing to the slightly changed molecular conformation after Cy-HPT is complexed with the albumin protein. Cy-HPT can be adsorbed onto the hydrophobic domain of HSA, the complex with much higher hydrophobicity can act as an “adhesive” between different proteins, and then induce assembly of more albumin proteins to form a nanoparticle, inside which Cy-HPT are embedded.<sup>48</sup> The satisfactory optical properties lay the foundation for the dyes to be used for bioimaging and tumor treatment.

#### 3.2 Evaluation Photothermal Conversion and Singlet Oxygen Generation Efficiency

We then evaluated their photoconverted thermal effects in detail. Under exposure to an 808 nm continuous NIR laser at 1.5 W/cm<sup>2</sup> for 5 min (Fig. 2a), the temperature of Cy-HPT (10  $\mu\text{M}$ ) and HSA@Cy-HPT (200  $\mu\text{g/mL}$ , containing equivalent 10  $\mu\text{M}$  of Cy-HPT) solutions rose from 24 °C to 45 °C and 55 °C, respectively. HSA@-



**Scheme 1.** The synthetic route and the photoinduced treatment mechanism of Cy-HPT and HSA@Cy-HPT.

Cy-HPT has larger photothermal conversion efficiency (54.98%) than Cy-HPT (45.21%). This is probably because 1) the absorption coefficient of HSA@Cy-HPT is 42% higher than that of Cy-HPT owing to the complex effect. 2) The photostability of HSA@Cy-HPT is dramatically increased. It has been reported that ICG decomposition due to the break of the double bonds under irradiation,<sup>51</sup> such phenomenon also occurs to our Cy-HPT. As shown in Fig. 2c, the color of Cy-HPT sample disappeared by five cycles of irradiation 808 nm 1.5 W/cm<sup>2</sup> 10 min due to similar double-bond breaking decomposition mechanism proved by analyzing the mass spectra of sample solution (m/z = 403.46, 429.73 and 964.44) and characterizing the structures of the decomposition products (Fig. S1). Cy-HPT is decomposed by the laser through the reaction of the double bonds of the flexible polymethine chain with photo-induced generated <sup>1</sup>O<sub>2</sub> by cycloaddition and finally thermal decomposition into carbonyl compounds.<sup>52, 53</sup> By contrast, as shown as Fig. 2b and 2c, the heating ability of HSA@Cy-HPT greatly increased, because the molecular conformation of Cy-HPT embedded in hydrophobic region of HSA was stabilized, preventing the occurrence of the oxidation-induced decomposition reaction. Thus, the photo-stability and photothermal ability of Cy-HPT in hybrid NPs are dramatically improved.

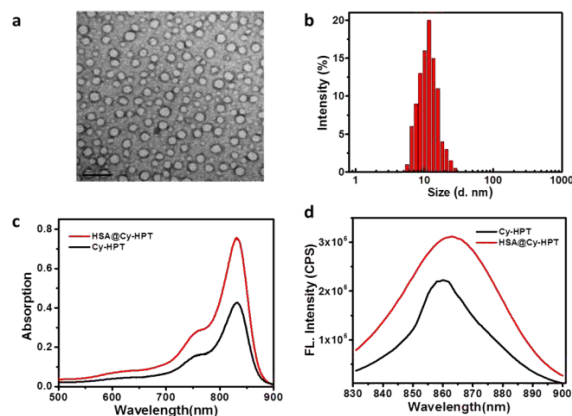


**Fig. 1** a) TEM imaging of HSA@Cy-HPT. Scale bar: 20 nm. b) The Hydrodynamic diameters of HSA@Cy-HPT measured by DLS. c) Absorption spectra of Cy-HPT and HSA@Cy-HPT. d) Fluorescence emission spectra of Cy-HPT and HSA@Cy-HPT.

Similar results can be found in living cells. As shown in Fig. 2d, the fluorescence signal of HSA@Cy-HPT in HepG2 cells exhibited stability after the laser irradiation for 30 min. By contrast, the fluorescence from Cy-HPT labeled cells apparently decreased within 10 min and totally disappeared after 30 min irradiation. This result suggested that HSA@Cy-HPT was suitable for long-term and repeated cancer treatment.

Furthermore, the singlet oxygen ( $^1O_2$ ) generated from Cy-HPT and HSA@Cy-HPT were also detected by using Singlet oxygen sensor green (SOSG, Invitrogen co., USA) as a probe. As shown in Fig. 2e, the emission intensity indicated that  $^1O_2$  was generated by Cy-HPT and HSA@Cy-HPT in the solution. However, the  $^1O_2$  production of HSA@Cy-HPT was higher than that in blank water and Cy-HPT. We also compared the  $^1O_2$  generation of Cy-HPT and HSA@Cy-HPT with indocyanine green (ICG), which is a

nontargeting clinically available heptamethine cyanine dye.<sup>54</sup> As shown in Fig. 2e, Cy-HPT and HSA@Cy-HPT exhibited more  $^1O_2$  generation than that of ICG. This finding is consistent with previous studies.<sup>16</sup> Next,  $^1O_2$  generation of Cy-HPT and HSA@Cy-HPT in cells upon NIR laser irradiation was also investigated. SOSG was employed to detect the generation of  $^1O_2$  in living cells by laser scanning confocal microscope. As shown in Fig. 2f, the control group showed weak fluorescence, indicating no  $^1O_2$  generated in blank cells. Both laser groups emitted fluorescence with prolonged irradiation time. And the signal from HSA@Cy-HPT treated cells is stronger. These imaging results convinced that HSA@Cy-HPT could generate more  $^1O_2$  in living cells under laser irradiation. These above results show the potential of Cy-HPT and HSA@Cy-HPT for PDT/PTT therapy.

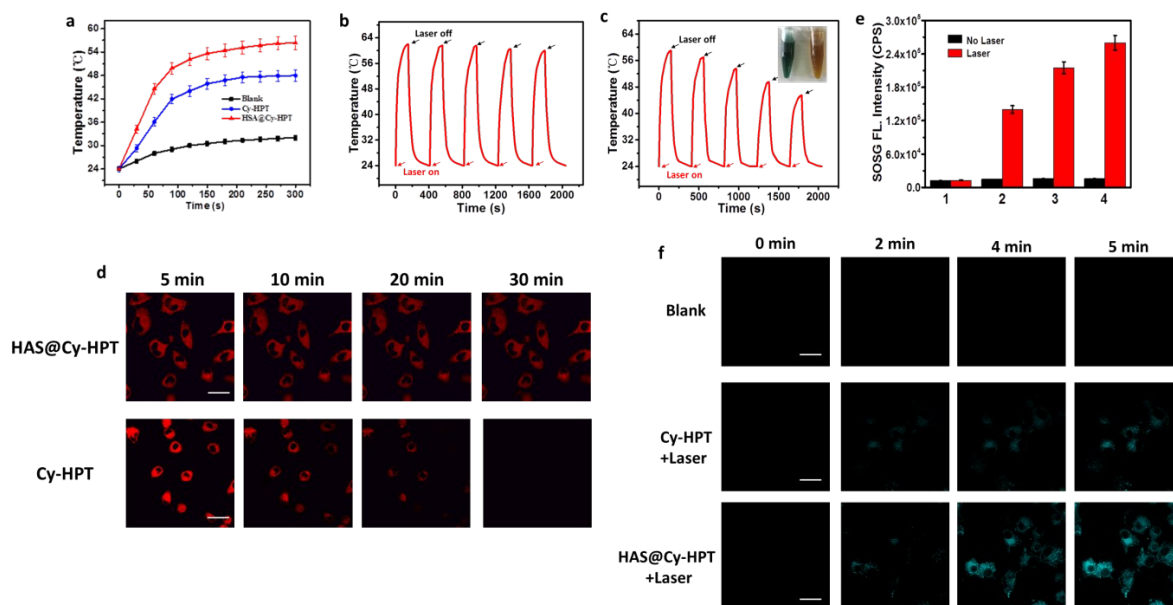


**Fig. 2** a) Temperature curves of Cy-HPT and HSA@Cy-HPT with during 5 min NIR laser irradiation. b) The photothermal stability of HSA@Cy-HPT. c) The photothermal stability of Cy-HPT. d) Confocal microscopy images of HepG2 cells for photothermal stability of Cy-HPT and HSA@Cy-HPT upon the continuous laser irradiated for 30 min. Fluorescence channel:  $\lambda_{ex} = 808$  nm,  $\lambda_{em} = 830 - 880$  nm. e) The fluorescence intensity of SOSG: 1. Blank, 2. ICG, 3. Cy-HPT, 4. HSA@Cy-HPT. f) Confocal microscopy images of HepG2 cells for evaluating the generation of  $^1O_2$  by SOSG upon NIR laser irradiation. Fluorescence channel:  $\lambda_{ex} = 490$  nm,  $\lambda_{em} = 510 - 560$  nm. Images are representative of  $n = 5$  independent experiments. Scale bar = 20  $\mu$ m.

### 3.3 In Vitro Photoinduced Cytotoxicity and Organelle Localization

We next tested the in vitro cancer cell killing efficacy of Cy-HPT and HSA@Cy-HPT. HepG2 cells originally obtained from the Committee on Type Culture Collection of Chinese Academy of Sciences (Shanghai, China) and cultured under recommended conditions, were incubated with free Cy-HPT and HSA@Cy-HPT for 72 h. The standard cell viability assay using 3-(4,5-dimethylthiazol-2-yl)-2,5-diphenyltetrazolium bromide (MTT) was then conducted. As demonstrated in Fig. 3a and 3b, above 72% (Cy-HPT) and 81% (HSA@Cy-HPT) of cells survived for tumor cells (HepG2 cells) after the cells were incubated with 10  $\mu$ M Cy-HPT or 200  $\mu$ g/mL HSA@Cy-HPT for 72 h, then the 50% cell survival concentration value ( $IC_{50}$ ) was predicted to be 32  $\mu$ M (Cy-HPT) and 826  $\mu$ g/mL (HSA@Cy-HPT) for HepG2 cells, respectively, which

indicated the low cytotoxicity of Cy-HPT and HSA@Cy-HPT under no laser irradiation.

On the basis of the above experiments, it is necessary to verify whether Cy-HPT and HSA@Cy-HPT has great potential to phototherapeutic effect in complex biological systems. First, we tested Cy-HPT and HSA@Cy-HPT for its PTT and PDT ability in tumor cells (HepG2 cells). MTT assay showed the cell viability in the radiation groups decreased with the increased concentration of Cy-HPT (0 - 10  $\mu$ M) and HSA@Cy-HPT (0 - 200  $\mu$ g/mL), and the cell viability rate obviously decrease at 10  $\mu$ M (Cy-HPT) and 200  $\mu$ g/mL (HSA@Cy-HPT) (Fig. 3a-3b). In contrast, the cell viability in the nonirradiation groups was not affected significantly. All these data enabled Cy-HPT and HSA@Cy-HPT exhibited an efficient PTT and PDT ability to kill tumor cells.

Nanoparticles can selectively enter into cancer cells via endocytosis by lysosomes.<sup>55</sup> Therefore, organelle co-localization experiment of HSA@Cy-HPT was investigated. As shown in Fig.

3c, HepG2 cells were able to uptake the HSA@Cy-HPT after 3 h of incubation. A large amount of HSA@Cy-HPT was observed to accumulate and colocalize with LysoTracker in the cells, indicating that the HSA@Cy-HPT could be taken up by cancer cells via endocytosis. Afterward, their endocytosis was further studied using an inhibitor. Chlorpromazine, an inhibitor of clathrin-mediated endocytosis,<sup>15</sup> was employed in HepG2 cells experiment. HepG2

cells were treated with chlorpromazine (15  $\mu\text{g}/\text{mL}$ ) for 1 h, then HSA@Cy-HPT, as as described in above experiment, was added to the cells for 3 h. As shown as Fig. 3d, an obviously faint fluorescence was exhibited in cells,  $\approx 40\%$  decreased in the cellular uptake of HSA@Cy-HPT, indicated that the nanoparticles were mainly internalized via endocytosis.

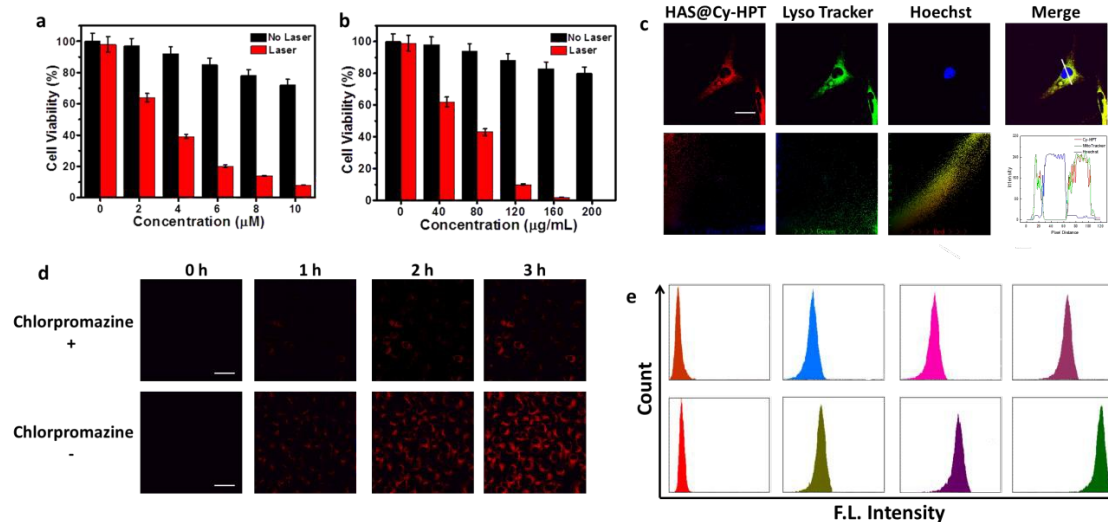


**Fig. 3** a), b) The cytotoxicity of a) Cy-HPT and b) HSA@Cy-HPT for HepG2 cells under no laser irradiation or laser irradiation. c) Lysosomes localization of HSA@Cy-HPT was determined by co-stained HSA@Cy-HPT with lysosomes trackers (Lyso Tracker) in HepG2 cells, the co-localization areas of the red and blue channels selected, the co-localization areas of the green and blue channels selected, the co-localization areas of the green and red channels selected and the intensity profile of regions of interest (white line in Merge) across cells. Red channel:  $\lambda_{\text{ex}} = 808 \text{ nm}$ ,  $\lambda_{\text{em}} = 830 - 880 \text{ nm}$ . LysoTracker showing lysosomes (green channel:  $\lambda_{\text{ex}} = 559 \text{ nm}$ ,  $\lambda_{\text{em}} = 570 - 650 \text{ nm}$ ). Hoechst showing nuclei (blue channel:  $\lambda_{\text{ex}} = 405 \text{ nm}$ ,  $\lambda_{\text{em}} = 425 - 525 \text{ nm}$ ). Images are representative of  $n = 5$  independent experiments. Scale bar:  $10 \mu\text{m}$ . d) Confocal microscopy images of HepG2 cells for the way of cellular uptake of HSA@Cy-HPT via endocytosis. Scale bar:  $40 \mu\text{m}$ . e) Flow cytometry assay of HepG2 cells correspond with d.

### 3.4 Cellular Uptake Kinetic and Cellular Selectivity

On the basis of the above fluorescence imaging experiments, the kinetic experiment of the cellular uptake of Cy-HPT and HSA@Cy-HPT was studied. By choosing HepG2 cells as cell models, the cells were treated with Cy-HPT ( $2 \mu\text{M}$ ) and HSA@Cy-HPT ( $40 \mu\text{g}/\text{mL}$ , containing equivalent  $2 \mu\text{M}$  of Cy-HPT), then subjected to cell fluorescence imaging by laser scanning confocal microscope at different time points. As shown as Fig. 4a, the cells were treated with Cy-HPT and HSA@Cy-HPT from 0 - 3 h, the fluorescence signal was became stronger over time indicated that the cellular uptake of Cy-HPT and HSA@Cy-HPT exhibited time-dependent mode. However, the fluorescence signal that treated with HSA@Cy-HPT for 3 h and Cy-HPT for 0.5 h reached the maximum value. This result demonstrates that Cy-HPT and HSA@Cy-HPT had the most intracellular accumulation after that treated for 0.5 h and 3 h, respectively. Support data the best accumulation time point of Cy-HPT and HSA@Cy-HPT for PDT and PTT in the tumor cells.

It has been reported that HSA NPs possess both passive and active tumor-targeting abilities via enhanced permeability and retention (EPR) effect and gp60 and SPARC receptor-mediated transcytosis, respectively.<sup>26</sup> In our study, the cellular uptake selectivity of the nanoparticles HSA@Cy-HPT was examined. HSA@Cy-HPT were added to both tumor cells (HepG2 cells) and normal cells (L02 cells) at  $37 \text{ }^\circ\text{C}$  and incubated for 3 h. As shown as Fig. 4b, only weak fluorescence signal was observed in L02 cells after 3 h of incubation.

The obvious difference in fluorescence intensities between cancer cells and normal cells suggested the cancer targeting capability of HSA@Cy-HPT. For comparison, the same experiments were performed with  $2 \mu\text{M}$  free Cy-HPT. There almost no obvious differences between tumor cells and normal cells (Fig. 4b). This is probably because the small-molecules enter cells mainly via non-specific free diffusion. The enhanced endocytosis of HSA@Cy-HPT by tumor cells was also verified by flow cytometry. The results were consistent with the cell fluorescence imaging. These results indicated that the nanoparticles HSA@Cy-HPT had a tumor targeting function without any tumor targeting ligand and enhanced uptake of HSA@Cy-HPT due to gp60 and SPARC receptor-mediated transcytosis.<sup>26</sup> This is beneficial to obtain ideal curative effect for real tumor treatment applications.

### 3.5 In Vitro Synergetic PDT, PTT Effect of HSA@Cy-HPT

To verify that the therapeutic effect of HSA@Cy-HPT were contributed by synergetic PDT and PTT treatments, laser irradiation toward HepG2 cells were performed under ice incubation for single PDT treatment or pretreated with N-acetylcysteine (NAC) and  $\text{NaN}_3$  to scavenge ROS and  $\text{O}_2$ <sup>56</sup> for single PTT treatment. When treated with HSA@Cy-HPT at 0, 40, 80, 120, 160, 200  $\mu\text{g}/\text{mL}$ , MTT assay showed that no cell viability was detected in both PTT and PDT treatment at 200  $\mu\text{g}/\text{mL}$  (HSA@Cy-HPT), 20.3% cell viability in PTT treatment alone, and 12.4% cell viability in PDT treatment

alone (Fig. 5a). The results suggest that the photoinduced cytotoxicity of HSA@Cy-HPT is synergistically enhanced by PDT and PTT combinatorial treatment and the treatment effect of HSA@Cy-HPT for tumor cells is effective. The phototoxicity of HSA@Cy-HPT was also intuitively confirmed through fluorescence images of Calcein AM and propidium iodide (PI) co-stained HepG2 cells (Fig. 5b). The green from Calcein AM and the red from PI showed the live and dead cells respectively, confirmed the synergistic effects of PDT and PTT. Flow cytometry with Annexin V-PE was tested to evaluate the apoptosis rate of single PTT, single PDT and synergistic PDT and PTT. After 3 h incubation with HSA@Cy-HPT at 200  $\mu\text{g/mL}$  and 5 min NIR light irradiation (808

nm, 1.5  $\text{W/cm}^2$ ), apoptotic ratios of synergistic PDT and PTT were observed with obvious increase than the single PTT or single PDT for HepG2 cells (Fig. 5c). Therefore, the cell death was mediated by the synergistic PDT and PTT of HSA@Cy-HPT manner. Heat shock protein 70 (Hsp70) is typically synthesized in response to heat stress to protect the cell for thermal or oxidative stress.<sup>57</sup> Thus, Hsp70 expression was monitored to evaluate the heat stress of cells. As shown in Fig. 5d, the Hsp70 expression was significantly increased with the PTT group and synergistic PDT and PTT group. Further indicating that cell apoptosis was mediated by the synergistic PDT and PTT of HSA@Cy-HPT.

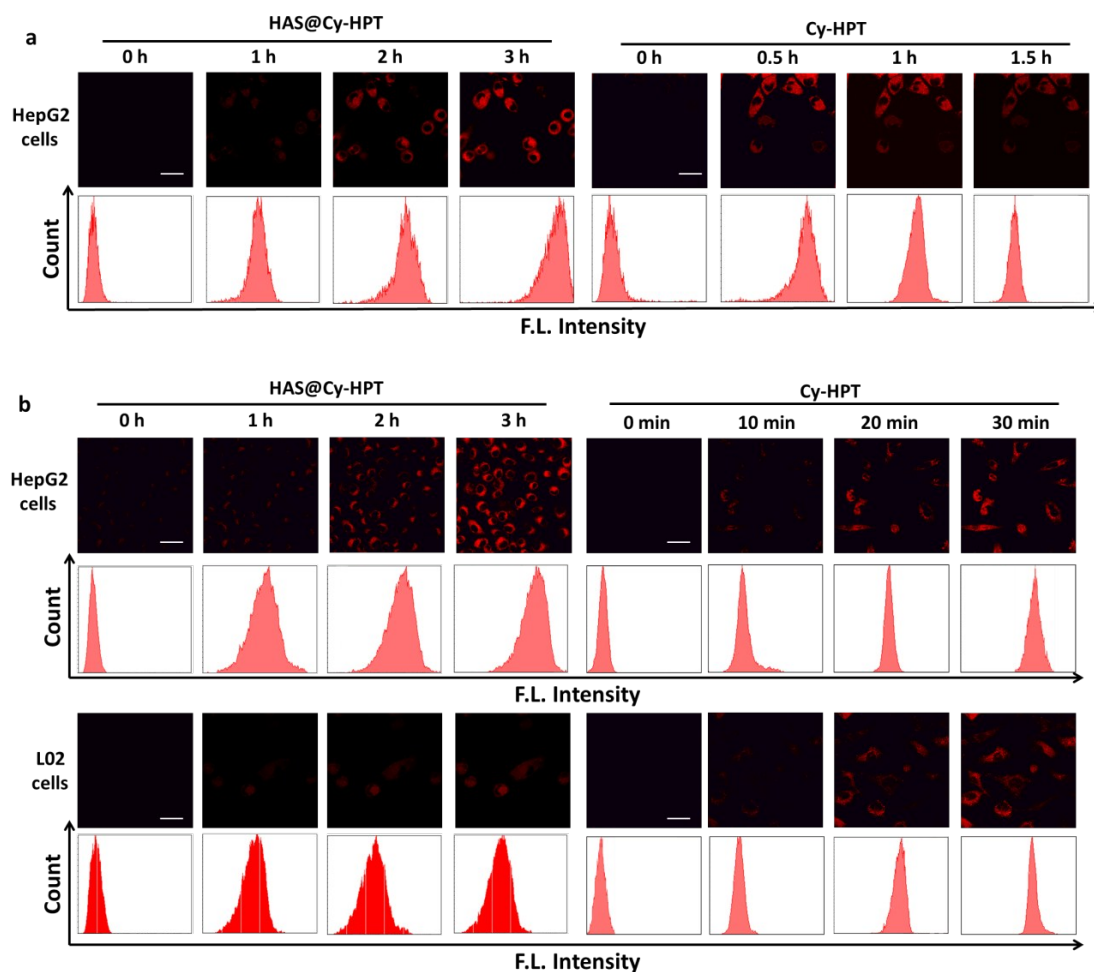


**Fig. 4** a) Confocal microscopy images and flow cytometry assay of HepG2 cells for the kinetic experiment of the cellular uptake of Cy-HPT and HSA@Cy-HPT. b) The selective cellular uptake of the HSA@Cy-HPT and free Cy-HPT in tumor cells (HepG2 cells) and normal cells (L02 cells). Fluorescence channel:  $\lambda_{\text{ex}} = 808$  nm,  $\lambda_{\text{em}} = 830 - 880$  nm. Images are representative of  $n = 5$  independent experiments. Scale bar = 20  $\mu\text{m}$ .

### 3.6. In Vivo NIR Fluorescent Imaging and Tumor-bearing Mice Imaging

HSA@Cy-HPT was chosen as the ideal PDT and PTT agent applied to mice and tumor xenograft models due to its excellent photothermal conversion ability and photodynamic properties. First, the application of HSA@Cy-HPT for fluorescence imaging *in vivo* was studied in BALB/c mice. Simultaneously, pharmacokinetics of HSA@Cy-HPT *in vivo* also was investigated, and Cy-HPT as the control. All experimental procedures were conducted in conformity

with institutional guidelines for the care and use of laboratory animals, and protocols were approved by the Institutional Animal Care and Use Committee in Binzhou Medical University, Yantai, China (Approval Number: No.BZ2014-102R). HSA@Cy-HPT (10 mg/kg) and Cy-HPT (5 mg/kg) were injected into BALB/c mice by intravenous (i.v.) injection. NIR fluorescent imaging was performed at different time points. As shown as Fig. 6a, a weak fluorescence signal was obtained at the beginning, then the fluorescence signal was becoming stronger and stronger with the passage of time. The strongest fluorescence signal (mainly in the liver) was obtained after

HSA@Cy-HPT was injected for 12 h, and for Cy-HPT after injected for 6 h, next the fluorescence signal was getting weaker due to the mice metabolism. And the main tissue and organ were removed by dissected, the fluorescence signal of ex vivo organs (heart, liver, spleen, lung, kidney) were analyzed by fluorescence imaging. High fluorescent contrast between liver and other normal tissue in BALB/c mice was observed, suggested that the liver preferential

accumulation of HSA@Cy-HPT due to the liver is a major metabolic site, and the obviously fluorescence signal was also obtained in kidney. The results revealed that the nanoparticles (HSA@Cy-HPT) not only could retain *in vivo* for a longer time than free Cy-HPT, but also had an efficient renal clearance to avoid the long-term risk of adverse effects.

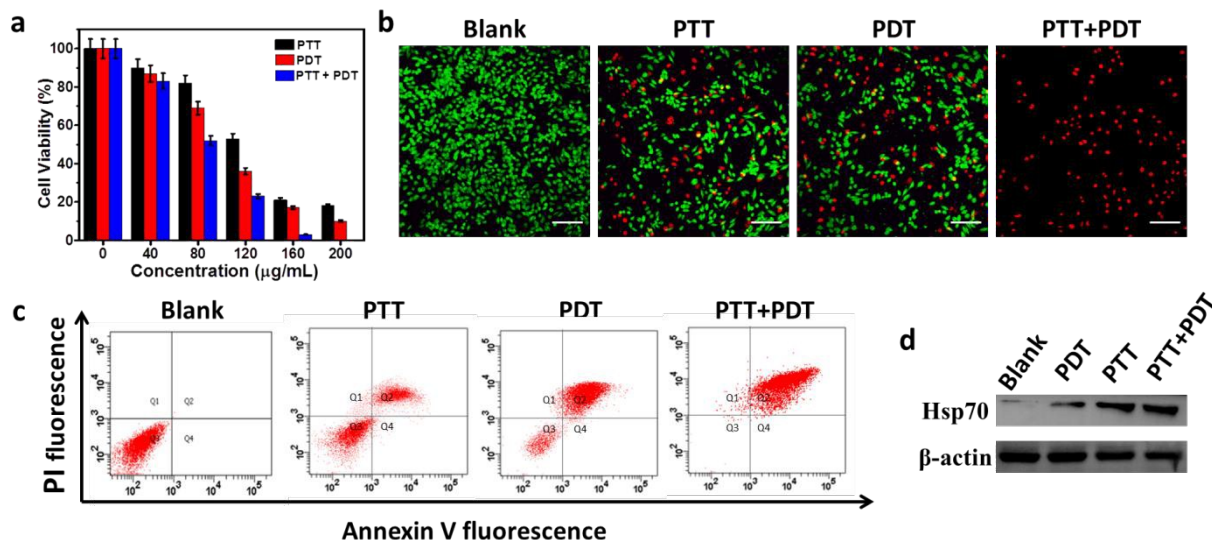


**Fig. 5** a) MTT assay of single PTT, single PDT and synergetic PDT and PTT of HSA@Cy-HPT for HepG2 cells under laser irradiation. b) Fluorescent images of Calcein AM/PI co-stained HepG2 cells after PTT, PDT, or synergetic PDT and PTT treatments with HSA@Cy-HPT. Scale bar: 60  $\mu\text{m}$ . c) Flow cytometry analysis of Annexin V-PE to evaluate the apoptosis rate of single PTT, single PDT and synergetic PDT and PTT. d) Western blotting analysis of Hsp70 of single PTT, single PDT and synergetic PDT and PTT,  $\beta$ -actin was used as a loading control.

Nanoparticles can preferentially accumulate in the tumor site through enhanced permeability and retention (EPR) effect without requiring chemical conjugation of tumor-targeting ligands have been recently identified and have shown unique properties for cancer *in vivo* imaging.<sup>46, 58</sup> In order to evaluate the cancer specificity of HSA@Cy-HPT, nude mice bearing HepG2 cell xenografts were established as described previously. HSA@Cy-HPT (10 mg/kg) intravenously into the nude mice bearing HepG2 cell tumor xenografts and then NIR fluorescent imaging was performed by PerkinElmer IVIS Lumina XRMS Series III In Vivo Imaging System. As shown as Fig. 6b, the fluorescence signal appeared in the location of liver after intravenous injection 0.5 h, then HSA@Cy-HPT was injected after 6 h, a strong fluorescence signal was obtained in the tumor tissue site. As our expected, the fluorescence signal in tumor site was continuous, and the effective fluorescence signal was still existed after 72 h. To further confirm the accumulation of HSA@Cy-HPT in tumor tissue site, the mice were sacrificed and their main organs including tumors were dissected. The ex vivo NIR imaging of the dissected organs from above models further confirmed its tumor preferential accumulation (Fig. 6b). The result demonstrated that HSA@Cy-HPT was an effective nano-reagent for tumor-targeted *in vivo*. And the long-time accumulation of HSA@Cy-HPT in tumor site was beneficial to the efficient of PDT and PTT.

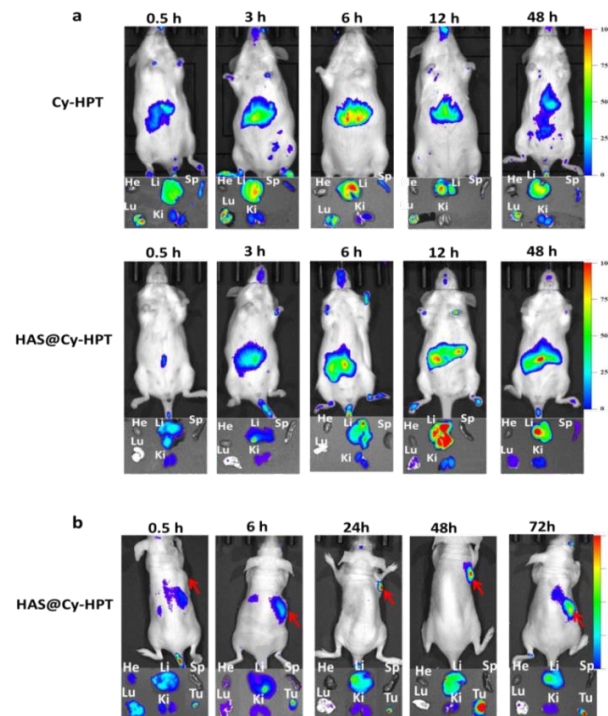


**Fig. 6** a) Cy-HPT and HSA@Cy-HPT for fluorescence imaging in BALB/c mice and ex vivo fluorescent imaging of dissected main organs in different time points. b) HSA@Cy-HPT for fluorescence imaging in subcutaneous HepG2 tumor model and ex vivo fluorescent imaging of dissected main organs in

different time points. He: heart; Li: liver; Sp: spleen; Lu: lung; Ki: kidney; Tu: tumor. Images displayed represent emission intensities collected window: 830 - 880 nm,  $\lambda_{\text{ex}} = 808$  nm. Data are presented as mean  $\pm$  SD (n = 5).

### 3.7 Thermal Images and Phototherapy in Xenograft Model

On the basis of the above experiments, *in vivo* phototherapeutic efficacy of HSA@Cy-HPT was initially elucidated in HepG2 subcutaneous tumor xenograft models. The tumor xenograft models were divided into four groups, PBS buffer solution was into the tumor xenograft models by intravenous injection as PBS nonirradiation group, the tumor xenograft models were injected PBS and exposure to an 808 nm continuous NIR laser at 1.5 W/cm<sup>2</sup> for 5 min at 24 h postinjection as PBS irradiation group, the tumor xenograft models were injected HSA@Cy-HPT (10 mg/kg) as

HSA@Cy-HPT nonirradiation group, the tumor xenograft models were injected HSA@Cy-HPT and exposure to an 808 nm continuous NIR laser at 1.5 W/cm<sup>2</sup> for 5 min at 24 h postinjection as HSA@Cy-HPT irradiation group. Then the tumor xenograft models were thermal imaged by Infrared Thermal Camera (TESTO 865) to monitor the real-time surface temperature of tumors at 24 h postinjection. As shown in Fig. 7a, the temperature of PBS irradiation group was increased to 43 °C after 5 min irradiation. As expected, the temperature of HSA@Cy-HPT irradiation group was reached up to near 60 °C after 5 min irradiation, which was high enough to ablate tumors.<sup>59</sup> Therefore, HSA@Cy-HPT has huge potential as a nano-reagent for efficient PTT therapy in tumor xenograft models.

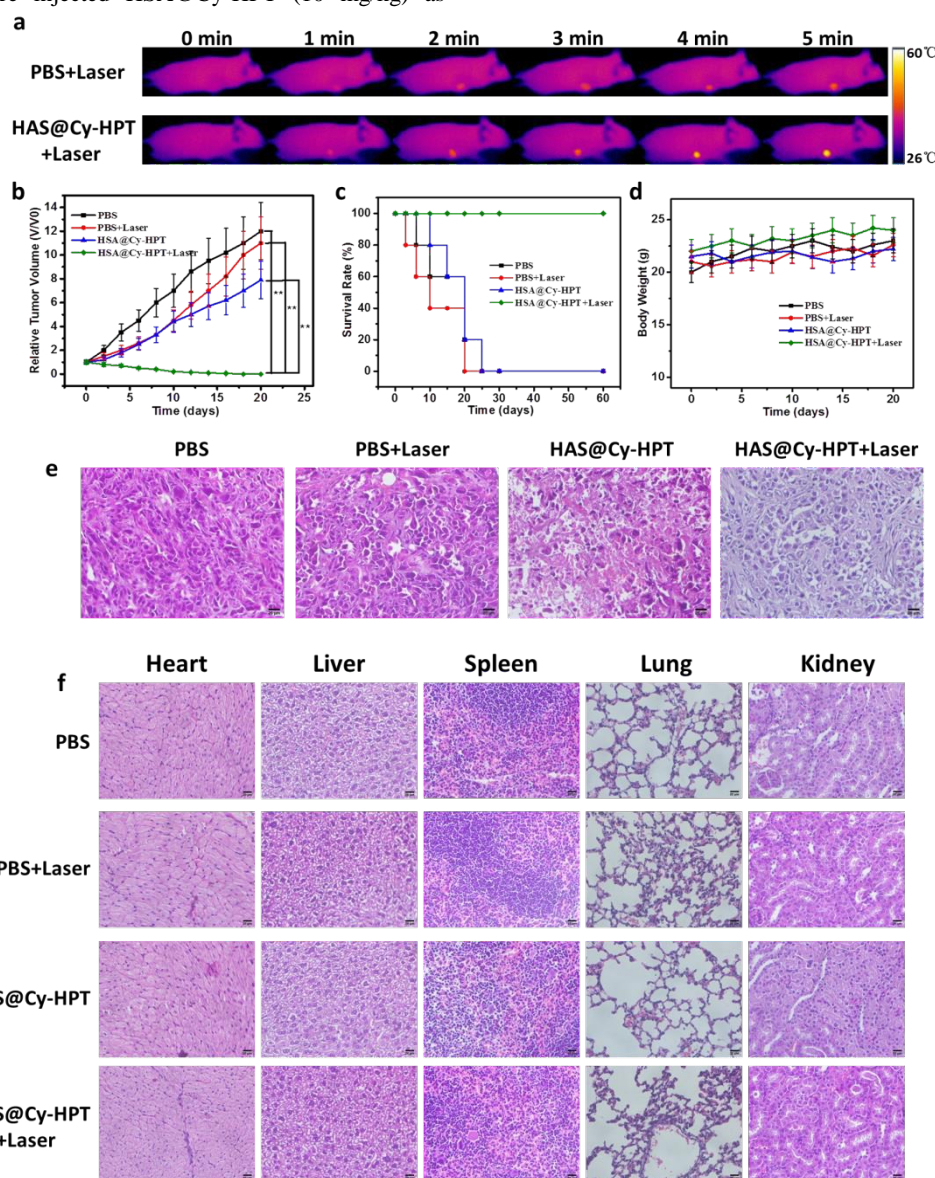


**Fig. 7** a) IR thermal images of subcutaneous HepG2 tumor xenograft mice during 5 min NIR laser irradiation. b) The relative tumor volume of subcutaneous HepG2 tumor xenograft mice in different groups. Statistical analysis was performed using the Student's *t*-test: \*\**p* < 0.01. c) The survival rate of HepG2 tumor xenograft mice in different groups. d) The body weight of HepG2 tumor xenograft mice in different groups. e) H&E staining of HepG2 tumor in different groups. Scale bar: 20  $\mu$ m. f) H&E staining of the normal tissues in different groups. Scale bar: 20  $\mu$ m. Magnification:  $\times$  400. Data are presented as mean  $\pm$  SD (n = 5).

To evaluate the inhibitory effect of HSA@Cy-HPT for tumor tissue in tumor xenograft models, the relative tumor volume were recorded for 20 d after treatment. The PBS nonirradiation group and PBS irradiation group all showed a  $\approx$ 12-fold increase in the tumor volumes, suggesting that the irradiation at 808 nm has no influence on tumor growth (Fig. 7b). And HSA@Cy-HPT nonirradiation group also exhibited a similar tumor growth in the absence of 808 nm irradiation, owing to its negligible cytotoxicity. Importantly, the HSA@Cy-HPT irradiation group resulted in a obviously tumor ablation without any regrowth under 808 nm irradiation (Fig. 7b). In addition, the survival rate was recorded for 60 d after treatment. Satisfactory, the survival rate of HSA@Cy-HPT irradiation group was maintained at 100%. The result demonstrated that HSA@Cy-HPT offers excellent PDT/PTT effect for inhibit tumor growth and extend survival rate.

To verify the anticancer efficacy of HSA@Cy-HPT under 808 nm laser irradiated, we further examined their tumor-damaging ability using the body weight of tumor xenograft models, as well as the hematoxylin & eosin (H&E) staining of tumor tissue and normal tissues. The body weight was a subtle decrease in the PBS irradiation groups in the first several days, and no significant difference for all groups at the end of observation period (Fig. 7d), suggesting the well-tolerance and unobvious photoinduced side effects of this treatment. For H&E staining, HSA@Cy-HPT irradiation group resulted in the destructive cell necrosis in the tumor at 6 h post-irradiation (Fig. 7e), indicating a severe cell injury. By contrast, PBS nonirradiation group, PBS irradiation group and HSA@Cy-HPT nonirradiation group had no distinct tumor damage regardless of irradiation. Moreover, HSA@Cy-HPT also caused no distinct damage against the normal tissues such as heart, liver, spleen, lung and kidney (Fig. 7f). Hence, it is clear that HSA@Cy-HPT precisely achieve potent photothermal damage against the tumors, synergized with photodynamic damage under 808 nm irradiated.

#### 4. Conclusions

In summary, we have developed a small molecule fluorophores Cy-HPT as a photosensitizer and a nanoparticle HSA@Cy-HPT as a tumor-targeted nano-photosensitive material. Cy-HPT and HSA@Cy-HPT all exhibited the excellent PDT/PTT effect *in vitro* and *in vivo*, and they could be metabolized in living mice within a reasonable time. However, the photothermal stability, photothermal conversion and generation of  $^1\text{O}_2$  of HSA@Cy-HPT were better than free Cy-HPT, and HSA@Cy-HPT have the long-time accumulation of in tumor site. These results suggesting that HSA@Cy-HPT could be serve as a tumor-targeted NIR imaging reagents *in vivo* for precise surgery. On the other hand, utilizing our formulated HSA@Cy-HPT, highly effectively combined PDT and PTT under the guidance of NIR imaging is conducted. Such treatment approach could not only result in obviously tumor ablation without any regrowth and extend survival rate of mice, but also offer significant therapeutic benefit in its minimal side effects in our study. Based on such biocompatible theranostic agent, it is hoped that imaging-guided combined PDT plus PTT would bring new hope to the future fight against cancer.

#### Conflicts of interest

There are no conflicts to declare.

#### Acknowledgements

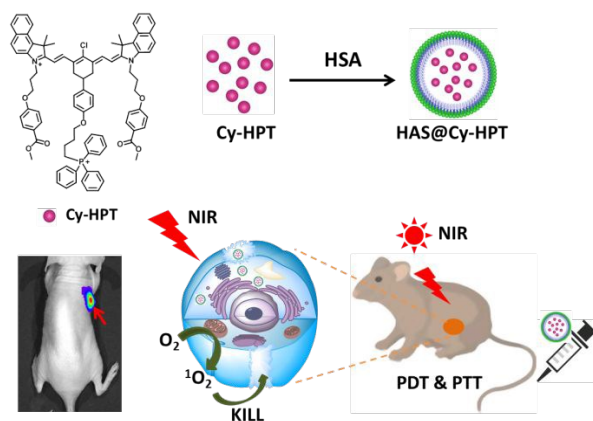
We thank the National Nature Science Foundation of China (Nos. 21575159, 81573393, 21575080), the program of Youth Innovation Promotion Association, CAS (Grant 2017256), the Instrument Developing Project of the Chinese Academy of Sciences (YZ201662).

#### References

- Cheng, L., Wang, C., Feng, L., Yang, K. and Liu, Z., *Chem Rev*, 2014, **114**, 10869-10939.
- Jaque, D., Martinez, M.L., Del, R.B., Haro-Gonzalez, P., Benayas, A., Plaza, J.L., Martin, R.E. and Garcia, S.J., *Nanoscale*, 2014, **6**, 9494-9530.
- Dolmans, D.E., Fukumura, D. and Jain, R.K., *Nat Rev Cancer*, 2003, **3**, 380-387.
- Agostinis, P., Berg, K., Cengel, K.A., Foster, T.H., Girotti, A.W., Gollnick, S.O., Hahn, S.M., Hamblin, M.R., Juzeniene, A., Kessel, D., Korbelik, M., Moan, J., Mroz, P., Nowis, D., Piette, J., Wilson, B.C. and Golab, J., *CA Cancer J Clin*, 2011, **61**, 250-281.
- Hilger, I., Rapp, A., Greulich, K.O. and Kaiser, W.A., *Radiology*, 2005, **237**, 500-506.
- Du Y, Jiang, Q., Beziere, N., Song, L., Zhang, Q., Peng, D., Chi, C., Yang, X., Guo, H., Diot, G., Ntziachristos, V., Ding, B. and Tian, J., *Adv Mater*, 2016, **28**, 10000-10007.
- Wang, S., Li, X., Chen, Y., Cai, X., Yao, H., Gao, W., Zheng, Y., An, X., Shi, J. and Chen, H., *Adv Mater*, 2015, **27**, 2775-2782.
- Zheng, M., Yue, C., Ma, Y., Gong, P., Zhao, P., Zheng, C., Sheng, Z., Zhang, P., Wang, Z. and Cai, L., *ACS Nano*, 2013, **7**, 2056-2067.
- Mauceri, H.J., Hanna, N.N., Beckett, M.A., Gorski, D.H., Staba, M.J., Stellato, K.A., Bigelow, K., Heimann, R., Gately, S., Dhanabal, M., Soff, G.A., Sukhatme, V.P., Kufe, D.W. and Weichselbaum, R.R., *Nature*, 1998, **394**, 287-291.
- Zhang, W., Guo, Z., Huang, D., Liu, Z., Guo, X. and Zhong, H., *Biomaterials*, 2011, **32**, 8555-8561.
- Park, H., Yang, J., Lee, J., Haam, S., Choi, I.H. and Yoo, K.H., *ACS Nano*, 2009, **3**, 2919-2926.
- Lane, D., *NAT Biotechnol*, 2006, **24**, 163-164.
- Wang, N., Zhao, Z., Lv, Y., Fan, H., Bai, H., Meng, H., Long, Y., Fu, T., Zhang, X. and Tan, W., *Nano Res*, 2014, **7**, 1291-1301.
- Luo, S., Tan, X., Fang, S., Wang, Y., Liu, T., Wang, X., Yuan, Y., Sun, H., Qi, Q. and Shi, C., *Adv Funct Mater*, 2016, **26**, 2826-2835.
- He, H., Ji, S., He, Y., Zhu, A., Zou, Y., Deng, Y., Ke, H., Yang, H., Zhao, Y., Guo, Z. and Chen, H., *Adv Mater*, 2017, **29**, 1606690-1606700.
- Tan, X., Luo, S., Long, L., Wang, Y., Wang, D., Fang, S., Ouyang, Q., Su, Y., Cheng, T. and Shi, C., *Adv Mater*, 2017, **29**, 1704196-1704205.
- Delaey, E., van Laar, F., De Vos, D., Kamuhabwa, A., Jacobs, P. and de Witte, P., *J Photochem Photobiol B*, 2000, **55**, 27-36.
- Kassab, K., *J Photochem Photobiol B*, 2002, **68**, 15-22.
- Yang, K., Xu, H., Cheng, L., Sun, C., Wang, J. and Liu, Z., *Adv Mater*, 2012, **24**, 5586-5592.

- 20 Meng, Z., Wei, F., Ma, W., Yu, N., Wei, P., Wang, Z., Tang, Y., Chen, Z., Wang, H. and Zhu, M., *Adv Funct Mater*, 2016, **26**, 8231-8242.
- 21 Patel, N., Pera, P., Joshi, P., Dukh, M., Tabaczynski, W.A., Sifers, K.E., Kryman, M., Cheruku, R.R., Durrani, F., Missert, J.R., Watson, R., Ohulchanskyy, T.Y., Tracy, E.C., Baumann, H. and Pandey, R.K., *J Med Chem*, 2016, **59**, 9774-9787.
- 22 Zheng, M., Li, Y., Liu, S., Wang, W., Xie, Z. and Jing, X., *ACS Appl Mater Interfaces*, 2016, **8**, 23533-23541.
- 23 Tian, J., Ding, L., Ju, H., Yang, Y., Li, X., Shen, Z., Zhu, Z., Yu, J.S. and Yang, C.J., *Angew Chem Int Ed Engl*, 2014, **53**, 9544-9549.
- 24 Sevick-Muraca, E.M., *ANNU REV MED*, 2012, **63**, 217-231.
- 25 Inoue, Y., Saiura, A., Arita, J. and Takahashi, Y., *Ann Surg*, 2015, **262**, e98-e99.
- 26 Sheng, Z., Hu, D., Zheng, M., Zhao, P., Liu, H., Gao, D., Gong, P., Gao, G., Zhang, P., Ma, Y. and Cai, L., *ACS Nano*, 2014, **8**, 12310-12322.
- 27 Jang, H.L., Zhang, Y.S. and Khademhosseini, A., *Nanomedicine (Lond)*, 2016, **11**, 1495-1497.
- 28 Conte, C., Maiolino, S., Pelloso, D.S., Miro, A., Ungaro, F. and Quaglia, F., *Top Curr Chem*, 2016, **370**, 61-112.
- 29 Lucky, S.S., Soo, K.C. and Zhang, Y., *Chem Rev*, 2015, **115**, 1990-2042.
- 30 Chen, W., Ouyang, J., Liu, H., Chen, M., Zeng, K., Sheng, J., Liu, Z., Han, Y., Wang, L., Li, J., Deng, L., Liu, Y. and Guo, S., *Adv Mater*, 2017, **29**, 1603864-1603871.
- 31 Park, J., Jiang, Q., Feng, D., Mao, L. and Zhou, H.C., *J Am Chem Soc*, 2016, **138**, 3518-3525.
- 32 Kim, J., Kim, J., Jeong, C. and Kim, W.J., *Adv Drug Deliv Rev*, 2016, **98**, 99-112.
- 33 Banerjee, S.R., Pullambhatla, M., Byun, Y., Nimmagadda, S., Foss, C.A., Green, G., Fox, J.J., Lupold, S.E., Mease, R.C. and Pomper, M.G., *Angew Chem Int Ed Engl*, 2011, **50**, 9167-9170.
- 34 West, J.L. and Halas, N.J., *Annu Rev Biomed Eng*, 2003, **5**, 285-292.
- 35 Huang, X., El-Sayed, I.H., Qian, W. and El-Sayed, M.A., *J Am Chem Soc*, 2006, **128**, 2115-2120.
- 36 Lim, E.K., Kim, T., Paik, S., Haam, S., Huh, Y.M. and Lee, K., *Chem Rev*, 2015, **115**, 327-394.
- 37 Chen, G., Roy, I., Yang, C. and Prasad, P.N., *Chem Rev*, 2016, **116**, 2826-2885.
- 38 Huang, J., Guo, M., Ke, H., Zong, C., Ren, B., Liu, G., Shen, H., Ma, Y., Wang, X., Zhang, H., Deng, Z., Chen, H. and Zhang, Z., *Adv Mater*, 2015, **27**, 5049-5056.
- 39 Song, X.R., Wang, X., Yu, S.X., Cao, J., Li, S.H., Li, J., Liu, G., Yang, H.H. and Chen, X., *Adv Mater*, 2015, **27**, 3285-3291.
- 40 Wang, Y., Yang, T., Ke, H., Zhu, A., Wang, Y., Wang, J., Shen, J., Liu, G., Chen, C., Zhao, Y. and Chen, H., *Adv Mater*, 2015, **27**, 3874-3882.
- 41 Lv, G., Guo, W., Zhang, W., Zhang, T., Li, S., Chen, S., Eltahan, A.S., Wang, D., Wang, Y., Zhang, J., Wang, P.C., Chang, J. and Liang, X.J., *ACS Nano*, 2016, **10**, 9637-9645.
- 42 Ng, K.K. and Zheng, G., *Chem Rev*, 2015, **115**, 11012-11042.
- 43 Gao, D., Gao, L., Zhang, C., Liu, H., Jia, B., Zhu, Z., Wang, F. and Liu, Z., *Biomaterials*, 2015, **53**, 229-238.
- 44 Qian, C., Yu, J., Chen, Y., Hu, Q., Xiao, X., Sun, W., Wang, C., Feng, P., Shen, Q.D. and Gu, Z., *Adv Mater*, 2016, **28**, 3313-3320.
- 45 Choi, H.S., Liu, W., Misra, P., Tanaka, E., Zimmer, J.P., Itty, I.B., Bawendi, M.G. and Frangioni, J.V., *Nat Biotechnol*, 2007, **25**, 1165-1170.
- 46 Zhou, C., Long, M., Qin, Y., Sun, X. and Zheng, J., *Angew Chem Int Ed Engl*, 2011, **50**, 3168-3172.
- 47 Liu, J., Wang, P., Zhang, X., Wang, L., Wang, D., Gu, Z., Tang, J., Guo, M., Cao, M., Zhou, H., Liu, Y. and Chen, C., *ACS Nano*, 2016, **10**, 4587-4598.
- 48 Chen, Q., Liang, C., Wang, C. and Liu, Z., *Adv Mater*, 2015, **27**, 903-910.
- 49 Chen, Q., Liang, C., Wang, X., He, J., Li, Y. and Liu, Z., *Biomaterials*, 2014, **35**, 9355-9362.
- 50 Huang, P., Rong, P., Jin, A., Yan, X., Zhang, M.G., Lin, J., Hu, H., Wang, Z., Yue, X., Li, W., Niu, G., Zeng, W., Wang, W., Zhou, K. and Chen, X., *Adv Mater*, 2014, **26**, 6401-6408.
- 51 Chen, J., Sheng, Z., Li, P., Wu, M., Zhang, N., Yu, X.F., Wang, Y., Hu, D., Zheng, H. and Wang, G.P., *Nanoscale*, 2017, **9**, 11888-11901.
- 52 Penha, F.M., Rodrigues, E.B., Maia, M., Meyer, C.H., Costa, E.P., Dib, E., Bechara, E., Lourenco, A., Lima, F.A., Freymuller, E.H. and Farah, M.E., *Ophthalmologica*, 2013, **230**, 59-67.
- 53 Engel, E., Schraml, R., Maisch, T., Kobuch, K., Konig, B., Szeimies, R.M., Hillenkamp, J., Baumler, W. and Vasold, R., *Invest Ophthalmol Vis Sci*, 2008, **49**, 1777-1783.
- 54 Polom, K., Murawa, D., Rho, Y.S., Nowaczyk, P., Hunerbein, M. and Murawa, P., *Cancer-AM Cancer Soc*, 2011, **117**, 4812-4822.
- 55 He, D., Hai, L., He, X., Yang, X. and Li, H., *Adv Funct Mater*, 2017, **27**, 1704089-1704101.
- 56 Friday, E., Koshy, N., Bhandari, V.K. and Torturro, F., *Blood*, 2010, **116**, 1475.
- 57 Chen, H., Adam, A., Cheng, Y., Tang, S., Hartung, J. and Bao, E., *Mol Med Rep*, 2015, **11**, 2276-2284.
- 58 Liu, J., Yu, M., Zhou, C., Yang, S., Ning, X. and Zheng, J., *J Am Chem Soc*, 2013, **135**, 4978-4981.
- 59 Perez-Hernandez, M., Del, P.P., Mitchell, S.G., Moros, M., Stepien, G., Pelaz, B., Parak, W.J., Galvez, E.M., Pardo, J. and de la Fuente, J.M., *ACS Nano*, 2015, **9**, 52-61.

## Table of Contents



A self-assembly nanoplateform of HSA@Cy-HPT for targeted near-infrared emission fluorescence imaging and effective phototherapy of cancer